

## Petroleum like biodiesel production by catalytic decarboxylation of oleic acid over Pd/Ce-ZrO<sub>2</sub> under solvent-free condition

Jae-Oh Shim<sup>a</sup>, Won-Jun Jang<sup>a</sup>, Kyung-Won Jeon<sup>a</sup>, Da-We Lee<sup>a</sup>, Hyun-Suk Na<sup>a</sup>, Hak-Min Kim<sup>a</sup>, Yeol-Lim Lee<sup>a</sup>, Seong-Yeun Yoo<sup>a</sup>, Byong-Hun Jeon<sup>b</sup>, Hyun-Seog Roh<sup>a,\*</sup>, Chang Hyun Ko<sup>c,\*</sup>

<sup>a</sup> Department of Environmental Engineering, Yonsei University, 1 Yonseidae-gil, Wonju, Gangwon, 26493, Republic of Korea

<sup>b</sup> Department of Natural Resources and Environmental Engineering, Hanyang University, 222 Wangsimni-ro, Seongdong-gu, Seoul, 04763, Republic of Korea

<sup>c</sup> School of Applied Chemical Engineering, Chonnam National University, 77 Yongbong-ro, Gwangju, 61186, Republic of Korea

### ARTICLE INFO

#### Keywords:

Oxygen vacancy  
Sustainable biodiesel  
Decarboxylation  
Solvent-free  
Ce/Zr ratio

### ABSTRACT

The Ce/Zr ratio of Pd/Ce-ZrO<sub>2</sub> catalysts was systematically changed in order to investigate the effect of oxygen vacancy concentration on their decarboxylation activity under solvent-free conditions for potential sustainable petroleum like biodiesel production. Pd/Ce<sub>0.5</sub>Zr<sub>0.5</sub>O<sub>2</sub> exhibited the highest catalytic activity from all other tested catalysts because it contained the highest oxygen vacancy concentration and Pd dispersion, as shown by the X-ray photoelectron spectroscopy, Raman spectroscopy, and CO-chemisorption data. A catalyst deactivation study also showed that both the Pd dispersion and the oxygen vacancy concentration influences the catalytic activity. The catalyst deactivation was found to occur mainly due to Pd sintering, decreases in the BET surface area and Pd dispersion, and partially due to the loss of oxygen vacancies.

### 1. Introduction

Extensive research has been carried out on the production of sustainable biodiesel from renewable resources in response to accelerating fossil fuel consumption and depletion, and to mitigate the effects of greenhouse gas emissions from fossil fuel combustion [1–5]. These issues have initiated studies on the conversion of biomass into biodiesel, which is produced from renewable sources such as plants and microalgae, making it a sustainable and carbon-neutral transport fuel [6,7].

First-generation biodiesel is commonly produced by transesterification, but must be blended with fossil fuels because its physical and chemical properties are less desirable than those of petroleum-derived diesel fuel [2,8–10]. The oxygenated compounds in biodiesel precursor must be eliminated to improve its physical and chemical properties. In this viewpoint, hydrodeoxygenation (HDO) process has been developed to overcome the drawbacks of first-generation biodiesel. The HDO process has advantage that the oxygen contents can be eliminated in the form of H<sub>2</sub>O, thus resultant product can retain carbon number and total energy contents [11]. However, HDO process requires excess amount of hydrogen that limits the economic feasibility of biodiesel production via HDO process [3]. Thus, catalytic decarboxylation of fatty acids was developed to overcome the above-mentioned limitation. The carboxylate group (COO<sup>-</sup>) of fatty acids (R-COOH) is removed as CO<sub>2</sub>

(R - COOH → R - H + CO<sub>2</sub>) to produce linear hydrocarbons that are similar to conventional petroleum-derived hydrocarbons [2,11,12].

Several researchers have found that H<sub>2</sub> is essential for the decarboxylation reaction, and that the reaction pathway changes depending on whether H<sub>2</sub> or N<sub>2</sub> atmospheres are used [2,13–15]. Immer et al. found that oleic acid is mainly decarboxylated in the presence of hydrogen, but inert conditions cause decarbonylation instead [2]. Arend et al. also reported that reaction condition is important for deoxygenation reaction [13]. Thus, proper amounts of H<sub>2</sub> should be required for the decarboxylation reaction.

Currently, catalysts based on various metals such as Pd, Pt, and Ni are used for the deoxygenation of fatty acids, and those based on palladium are the most effective catalysts for these reactions [1,2,11,13,14,16–28]. Murzin and co-workers reported that Pd has the highest catalytic activity in deoxygenation reactions at 300 °C [11]. They also reported that the catalytic activity of monometallic catalysts with various active metals decreases in the following order: Pd > Pt > Ni > Rh > Ir > Ru > Os [11]. Recent reports have shown that Pd-based catalysts for fatty acid decarboxylation are highly sensitive to the effects of the catalyst support, which plays a vital role in controlling the decarboxylation reaction pathway [29]. Ford et al. reported that a carbon-supported Pd catalyst was more active than SiO<sub>2</sub>- and Al<sub>2</sub>O<sub>3</sub>-supported Pd catalysts [29]. In addition, Pd/C catalysts

\* Corresponding authors.

E-mail addresses: [hsroh@yonsei.ac.kr](mailto:hsroh@yonsei.ac.kr) (H.-S. Roh), [chko@jnu.ac.kr](mailto:chko@jnu.ac.kr) (C.H. Ko).

<https://doi.org/10.1016/j.apcata.2018.07.005>

Received 21 March 2018; Received in revised form 22 June 2018; Accepted 2 July 2018

Available online 08 July 2018

0926-860X/ © 2018 Elsevier B.V. All rights reserved.

predominantly proceed via a decarboxylation route, whereas Pd/SiO<sub>2</sub> catalysts primarily give deoxygenation via decarbonylation. Recently, reducible oxides such as CeO<sub>2</sub>, TiO<sub>2</sub>, and ZrO<sub>2</sub> have been used in deoxygenation reactions [17,20,22,30]. According to the literature, carboxylic acids first adsorb at oxygen defect sites in the oxides, followed by elimination of the carboxyl group [20,22]. Thus, we have assumed that the concentration of oxygen vacancies affects the decarboxylation reaction.

The incorporation of another cation, such as Zr<sup>4+</sup>, in the CeO<sub>2</sub> lattice is known to enhance the creation of oxygen vacancies [31–34]. Our previous study also reveals that the insertion of Zr<sup>4+</sup> in the CeO<sub>2</sub> lattice enhances the redox properties and thermal resistance of CeO<sub>2</sub>, and the Ce/Zr ratio is well known to affect the physical and chemical properties of Ce-ZrO<sub>2</sub> mixed oxide supports [17,30,31,35]. The main purpose of our previous study is to increase the catalytic performance of Ce-ZrO<sub>2</sub> based catalysts by introducing small amount of hydrogen (1 bar, 20 vol.%) to maintain and activate the active sites of catalyst [17,30]. We designed a Pd-doped Ce-ZrO<sub>2</sub> catalyst with various Ce/Zr ratio for decarboxylation reactions to investigate the relationship between the concentration of oxygen vacancies and catalytic activity in a decarboxylation reaction, which was carried out at 300 °C.

Generally, deoxygenation reaction has been carried out in various solvent such as dodecane and toluene. From an economic view point, employment of auxiliary reagent could significantly raise the cost of the total biodiesel processing. Therefore, we have designed deoxygenation reaction under solvent free condition. The physical and chemical properties of Pd-doped Ce-ZrO<sub>2</sub> catalysts with various Ce/Zr ratios were characterized using various techniques, including Brunauer-Emmett-Teller (BET) surface area, X-ray diffraction (XRD), X-ray photoelectron spectroscopy (XPS), Ramanspectroscopy, and CO-chemisorption. The characterization data for each catalyst was correlated with its decarboxylation activity under solvent-free conditions.

## 2. Experimental

### 2.1. Catalyst preparation

Ce-ZrO<sub>2</sub> supports were prepared by a co-precipitation method using a solution of KOH (15 wt.%) as the precipitating agent, as reported in our earlier work [30,32–35]. Stoichiometric quantities of zirconyl nitrate solution (20 wt.% ZrO<sub>2</sub> basis, MEL Chemicals) and Ce(NO<sub>3</sub>)<sub>3</sub>·6H<sub>2</sub>O (99%, Aldrich) were combined in distilled water. The Ce/Zr atomic ratios were 4:1, 1:1, and 1:4 for Ce<sub>0.8</sub>Zr<sub>0.2</sub>O<sub>2</sub>, Ce<sub>0.5</sub>Zr<sub>0.5</sub>O<sub>2</sub>, and Ce<sub>0.2</sub>Zr<sub>0.8</sub>O<sub>2</sub>, respectively. The precipitates were aged at 80 °C for 3 days before they were washed five times with distilled water and then air-dried for 1 day at 110 °C. The prepared Ce-ZrO<sub>2</sub> supports were calcined in air atmosphere from room temperature to 500 °C at a heating rate of 1 °C/min, after which the final temperature was maintained for 6 h. Pd (Pd loading: 1 wt.%) was loaded by an incipient wetness impregnation method. Pd(NO<sub>3</sub>)<sub>2</sub> (99.999%, Aldrich) was used as a precursor. The Pd-loaded Ce-ZrO<sub>2</sub> catalysts were also calcined at 500 °C for 6 h.

### 2.2. Characterization

The BET surface area of the catalysts was measured using a nitrogen adsorption technique on an ASAP 2010 (Micromeritics) accelerated surface area and porosimetry instrument. Before analysis, the samples were degassed for 12 h at 110 °C under a vacuum less than 0.5 mm Hg. XRD was carried out using a Rigaku D/MAX-IIIC diffractometer operated at 40 kV and 100 mA with Ni-filtered Cu-Kα radiation. Lattice parameters were calculated from XRD peaks using Bragg's law. CO-chemisorption was conducted in an AutoChem 2920 instrument (Micromeritics). Temperature-programmed desorption of ammonia (NH<sub>3</sub> – TPD) was carried out to evaluate the total acidity of the catalysts using an Autochem 2920 instrument. The Pd dispersion was calculated

by assuming the adsorption stoichiometry of one CO per Pd surface atom (CO/Pd<sub>s</sub> = 1) [36]. The palladium dispersion (*D* (%)), metallic surface area (*S*<sub>Pd</sub> (m<sup>2</sup>/g)), and active Pd particle size (nm) of the catalysts were calculated using the following the equations:

$$D (\%) = \frac{V_s \times SF \times M_{Pd}}{W_s \times W_f \times V_{m,STP}} \times 100$$

$$S_{Pd} (m^2/g_{Pd}) = \frac{V_s \times SF \times N_A \times S_C}{W_s \times W_f \times V_{m,STP}}$$

$$\text{Active Pd particle size (nm)} = \frac{6 \times M_{Pd}}{W_s \times W_f \times \rho_{Pd} \times N_A \times S_{Pd}}$$

where *V*<sub>s</sub> represents the volume of sorbed H<sub>2</sub> (mL) under standard temperature and pressure (STP) conditions, *SF* is the stoichiometry factor (1), *M*<sub>Pd</sub> is the gram molecular weight of Pd (106.42 g/mol), *W*<sub>s</sub> represents the sample weight (g), *W*<sub>f</sub> is the weight fraction of Pd in the catalyst (1%), *V*<sub>m,STP</sub> is the molar volume of H<sub>2</sub> (22,414 mL/mol) under STP conditions, *N*<sub>A</sub> is the Avogadro's number (6.023 × 10<sup>23</sup>/mol), *S*<sub>C</sub> represents the cross sectional area of Pd (7.87 × 10<sup>-20</sup> m<sup>2</sup>), and *ρ*<sub>Pd</sub> is the density of Pd (12.02 g/cm<sup>3</sup>).

XPS spectra were obtained using a Kα spectrophotometer (VG Multilab 2000) with a high-resolution monochromator. The pressure of the analysis chamber was maintained at 6.8 × 10<sup>-9</sup> mbar. The detector was used in constant energy mode with a pass energy of 100 eV for the survey spectrum and 50 eV for the detailed scan. Binding energies were calibrated against the C 1s transition, which appeared at 284.6 eV. Raman spectra were obtained using a LabRam Aramis (Horiba Jobin Yvon) with excitation at 532 from a Nd-YAG laser. A 500 μm pinhole was used for a spectral resolution grating, yielding approximately 1.5 cm<sup>-1</sup> resolution. The concentration of oxygen vacancies (*N*) was calculated using the spatial correlation model from the relationship between correlation length (*L*) and grain size (*d*<sub>g</sub>) [37,38]. The detailed equation used was as follows:

$$d_g (\text{nm}) = \frac{51.8}{(\Gamma - 5)}$$

$$L (\text{nm}) = \sqrt[3]{\left(\frac{\alpha}{2d_g}\right)^2 \left[(d_g - 2\alpha)^3 + 4d_g^2\alpha\right]}$$

$$N = \frac{3}{4\pi L^3}$$

where *Γ* is the half-width at half-maximum (HWHM) of the Raman line (around 450 cm<sup>-1</sup>) broadening, and *α* is the radius of CeO<sub>2</sub> units (0.34 nm), determined from universal constants [37,38]. Oxygen content was measured by elementary analysis using a Thermo Finnigan FLASH EA-1112 Elemental Analyzer (EA).

### 2.3. Catalytic reaction

Decarboxylation reactions were carried out in an autoclave reactor (100 mL capacity) operating in batch mode. The temperature was measured using a K-type thermocouple. In a typical batch experiment, 27.5 g of oleic acid and 1.35 g of catalyst (reactant/catalyst = 20/1 w/w) were placed in the reactor. The Pd/Ce-ZrO<sub>2</sub> catalysts were reduced in 10% H<sub>2</sub>/N<sub>2</sub> atmosphere under a pressure of 1 atm at 200 °C (heating rate: 2.9 °C/min) for 2 h using a tubular furnace. The inlet reduction gas flow rate was 100 mL/min. Passivation process using 2% O<sub>2</sub>/N<sub>2</sub> at room temperature for 12 h was followed before the exposure to air to avoid explosive oxidation of reduced Pd/Ce-ZrO<sub>2</sub> catalyst. After oleic acid and the reduced Pd/Ce-ZrO<sub>2</sub> catalyst were loaded into the reactor, the reactor was flushed with nitrogen to remove any remaining oxygen. Then, the reactor was purged with pure hydrogen, and the pressure was increased to 20 bar. The reactor was heated from room temperature to 300 °C at a heating rate of 4.5 °C/min, and the reaction temperature was

maintained for 3 h. A multi-blade impeller mixed the liquid reactant and solid catalyst and the stirring speed was fixed at 300 rpm during the reaction. The reactor was subsequently cooled down to room temperature. The liquid products were collected after filtering the solid phase catalysts from the mixture. The used catalyst was collected, washed with 100 mL of toluene, and air-dried for 1 day at room temperature to test the stability of the Pd/Ce<sub>0.5</sub>Zr<sub>0.5</sub>O<sub>2</sub> catalyst. The liquid products were analyzed using gas chromatography (HP 6890 N) with a flame ionization detector and a capillary column (HP-5, 30 m). The product gas from the batch reactor was sampled to 0.5 L Tedlar bag (CEL Scientific Corp.) and it was analyzed by an online micro-gas chromatograph (Agilent 3000) equipped with molecular sieve and PLOT U columns. The conversion of oleic acid and the selectivity of C<sub>i</sub> products were calculated using the following equations (*n* : mole of compound, *i* : carbon number).

$$\text{Oleic acid conversion (\%)} = \frac{n_{\text{Oleic acid, in}} - n_{\text{Oleic acid, out}}}{n_{\text{Oleic acid, in}}} \times 100$$

$$C_i \text{ selectivity (\%)} = \frac{n_{C_i}}{n_{\text{Oleic acid, in}} - n_{\text{Oleic acid, out}}} \times 100$$

### 3. Results and discussion

#### 3.1. Catalyst characterization

Table 1 summarizes the characteristics of Pd/Ce-ZrO<sub>2</sub> catalysts with various Ce/Zr ratios. The BET surface area decreased with increasing Ce content: a phenomenon that has been well documented in related literature [30,39]. As a result, the Pd/Ce<sub>0.8</sub>Zr<sub>0.2</sub>O<sub>2</sub> catalyst showed the lowest BET surface area (45 m<sup>2</sup>/g). The BET surface area of the Pd/Ce-ZrO<sub>2</sub> catalysts with various Ce/Zr ratios decreased in the following order: Pd/Ce<sub>0.2</sub>Zr<sub>0.8</sub>O<sub>2</sub> (197 m<sup>2</sup>/g) > Pd/Ce<sub>0.5</sub>Zr<sub>0.5</sub>O<sub>2</sub> (122 m<sup>2</sup>/g) > Pd/Ce<sub>0.8</sub>Zr<sub>0.2</sub>O<sub>2</sub> (45 m<sup>2</sup>/g).

The Pd dispersion of the prepared catalysts was calculated from pulse CO chemisorption results. The Pd dispersion value of Pd/Ce-ZrO<sub>2</sub> catalysts with various Ce/Zr ratios is also summarized in Table 1. The Pd dispersion values ranged from 44% to 67%, with the Pd/Ce<sub>0.5</sub>Zr<sub>0.5</sub>O<sub>2</sub> catalyst exhibiting the highest value (67%) and the Pd/Ce<sub>0.2</sub>Zr<sub>0.8</sub>O<sub>2</sub> catalyst having the lowest (44%). As a result, the Pd/Ce<sub>0.5</sub>Zr<sub>0.5</sub>O<sub>2</sub> catalyst had the smallest active Pd particle size (1.7 nm) while the Pd/Ce<sub>0.2</sub>Zr<sub>0.8</sub>O<sub>2</sub> catalyst had the largest (2.6 nm). Simakova et al. reported that Pd catalysts with different Pd dispersion could show different catalytic activity and product distributions in the deoxygenation of mixtures of stearic acid and palmitic acid [26]. Pd catalysts with a high metal dispersion have higher catalytic activity than those with low Pd dispersion.

XRD patterns of the various Pd/Ce-ZrO<sub>2</sub> catalysts are shown in Fig. 1, and the lattice parameters of the Pd/Ce-ZrO<sub>2</sub> catalysts with various Ce/Zr ratios are summarized in Table 1. The diffractogram of Pd/Ce<sub>0.8</sub>Zr<sub>0.2</sub>O<sub>2</sub> shows peaks corresponding to cubic CeO<sub>2</sub> [30,31,40]. The main peaks shifted to higher angles and the lattice parameter of CeO<sub>2</sub> decreased slightly with increasing in Zr content because of the

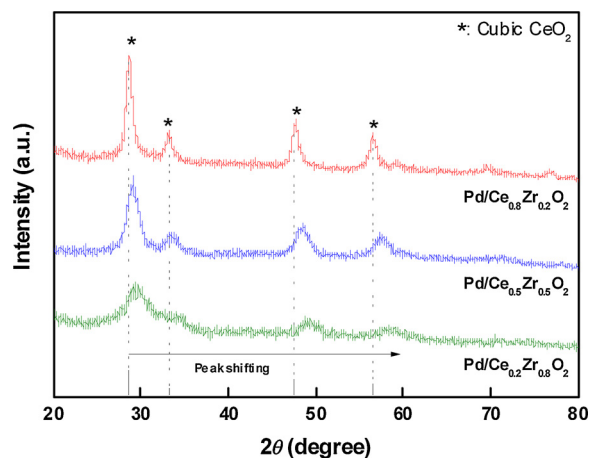


Fig. 1. XRD patterns of Pd/Ce-ZrO<sub>2</sub> catalysts with various Ce/Zr ratios.

relatively small atomic size of Zr<sup>4+</sup> (0.84 Å) compared to the atomic size of Ce<sup>4+</sup> (0.97 Å) [32]. In addition, the reported lattice parameter of pure CeO<sub>2</sub> is 0.5409 nm [41]. According to the literature, the structure of the Ce-ZrO<sub>2</sub> support depends on its composition [39]. When the Ce content is below 50%, the Ce-ZrO<sub>2</sub> supports adopt a tetragonal structure (Pd/Ce<sub>0.2</sub>Zr<sub>0.8</sub>O<sub>2</sub>), whereas a cubic Ce-ZrO<sub>2</sub> structure is formed when the Ce content is above 50% (Pd/Ce<sub>0.8</sub>Zr<sub>0.2</sub>O<sub>2</sub> and Pd/Ce<sub>0.5</sub>Zr<sub>0.5</sub>O<sub>2</sub>) [39]. No peaks corresponding to Pd metal were detected in any of the catalysts because the size of the Pd metal particles was less than 3 nm in all catalysts (highly dispersed), which is below the limit for X-ray line broadening analysis [42]. An XPS survey scan (Fig. S1), carried out to check for the presence of Pd species on the catalyst surface, confirmed the presence of metallic Pd species on the catalyst surface. Thus, the Pd nanoparticles were finely distributed on the Ce-ZrO<sub>2</sub> supports.

The O 1s spectra of Pd/Ce-ZrO<sub>2</sub> catalysts with various Ce/Zr ratios are shown in Fig. 2. Three types of oxygen species were detected in the XPS spectra, labeled as O<sub>L</sub>, O<sub>D</sub>, and O<sub>H</sub>, respectively [38]. The O<sub>L</sub>, O<sub>D</sub>, and O<sub>H</sub> peaks at 528.7 ± 0.4, 530.1 ± 0.4, and 531.7 ± 0.2 eV correspond to the lattice oxygen in Ce-ZrO<sub>2</sub> mixed oxide, oxygen vacancies, and adsorbed oxygen species from hydroxyl or water species on the metal surface, respectively [38]. When the Zr contents were increased in the Ce-ZrO<sub>2</sub> mixed oxide, all peaks shifted to higher binding energy (BE) because Zr<sup>4+</sup> is more electronegative than Ce<sup>4+</sup> [43]. The quantitative XPS elemental analysis of the O 1s peak of the various Pd/Ce-ZrO<sub>2</sub> catalysts are summarized in Table 1. The Pd/Ce<sub>0.5</sub>Zr<sub>0.5</sub>O<sub>2</sub> catalyst had the highest surface defect oxygen ratio of the prepared catalysts, of ~46.2%. Our hypothesis that the concentration of oxygen vacancies affects the decarboxylation reaction is based on the report by Peng et al. that carboxylic acids are reduced to aldehydes by the adsorption of the oxygen atoms of the carboxylic acid at the oxygen vacancies on the surfaces of reducible oxides (CeO<sub>2</sub>, TiO<sub>2</sub>, ZrO<sub>2</sub>), and the fact that adsorbed carboxylic acids can be converted to carboxylates followed by reaction with activated H<sub>2</sub>, which is activated through dissociative adsorption at oxygen defect sites [20]. Thus, we would

Table 1  
Characteristics of Pd/Ce-ZrO<sub>2</sub> catalysts with varying Ce/Zr ratio.

Catalysts	BET S.A. (m <sup>2</sup> /g) <sup>a</sup>	Pd dispersion (%) <sup>b</sup>	Active Pd particle size (nm) <sup>b</sup>	Lattice parameter (nm) <sup>c</sup>	O <sub>D</sub> / (O <sub>L</sub> + O <sub>D</sub> + O <sub>H</sub> )	Concentration of oxygen vacancies (cm <sup>-3</sup> )
Pd/Ce <sub>0.8</sub> Zr <sub>0.2</sub> O <sub>2</sub>	45	60	1.9	0.5385	34.2%	4.63 × 10 <sup>21</sup>
Pd/Ce <sub>0.5</sub> Zr <sub>0.5</sub> O <sub>2</sub>	122	67	1.7	0.5327	46.2%	6.06 × 10 <sup>21</sup>
Pd/Ce <sub>0.2</sub> Zr <sub>0.8</sub> O <sub>2</sub>	197	44	2.6	0.5268	29.6%	N.A. <sup>d</sup>

<sup>a</sup> Estimated from N<sub>2</sub> adsorption at -196 °C.

<sup>b</sup> Estimated from CO-chemisorption.

<sup>c</sup> Lattice parameter calculated from XRD peaks by Bragg's law.

<sup>d</sup> Not available due to very broad and weak Raman spectra.

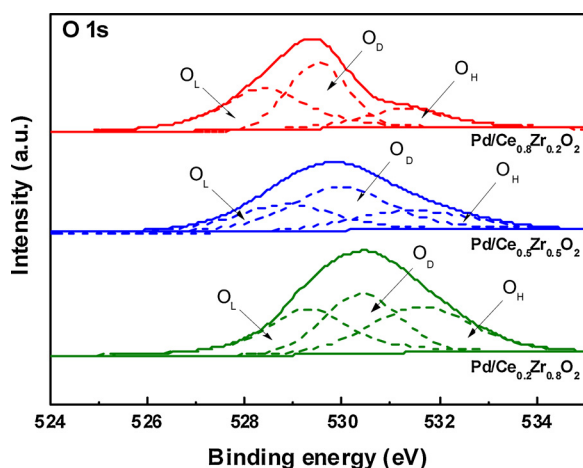


Fig. 2. O 1sXPS spectra of Pd/Ce-ZrO<sub>2</sub> catalysts with various Ce/Zr ratios.

expect that concentration of oxygen vacancies affects the decarboxylation reaction, and expect that the Pd/Ce<sub>0.5</sub>Zr<sub>0.5</sub>O<sub>2</sub> catalyst should have a higher activity than the others.

Raman spectroscopy analysis was carried out (Fig. 3) to confirm the structure and concentration of oxygen vacancies. Except for the Pd/Ce<sub>0.2</sub>Zr<sub>0.8</sub>O<sub>2</sub> catalyst, the catalysts showed a single Raman band at 448–462 cm<sup>-1</sup>, which was attributed to the F<sub>2g</sub> vibration mode of the fluorite structure of CeO<sub>2</sub> [38,43–48]. This peak shifted to lower wave number with the addition of Zr, since the addition of the smaller Zr<sup>4+</sup> (0.84 Å) caused local structure distortions in the CeO<sub>2</sub> lattice [38]. This result agreed with measurements of the lattice parameters. When the Ce/Zr ratio was decreased to 1/4 (as in the Pd/Ce<sub>0.2</sub>Zr<sub>0.8</sub>O<sub>2</sub> catalyst), this peak became weak and disappeared. This change indicates the disappearance of the cubic fluorite structure phase [49,50]. The concentration of oxygen vacancies can be calculated from the Raman band at 448–462 cm<sup>-1</sup>, and Table 1 shows the calculated concentrations of oxygen vacancies for the various Pd/Ce-ZrO<sub>2</sub> catalysts [37,38]. The Pd/Ce<sub>0.8</sub>Zr<sub>0.2</sub>O<sub>2</sub> catalyst had an oxygen vacancy concentration of  $4.63 \times 10^{21}$  cm<sup>-3</sup>. An increase in the oxygen vacancy concentration was observed when the Zr content increased to 50%, and the Pd/Ce<sub>0.5</sub>Zr<sub>0.5</sub>O<sub>2</sub> catalyst exhibited the highest concentration of oxygen vacancies. Calculation of the oxygen vacancy concentration of Pd/Ce<sub>0.2</sub>Zr<sub>0.8</sub>O<sub>2</sub> catalyst was not possible because of the broad and weak Raman spectra. However, we can infer from previous XPS quantitative elemental analyses that the oxygen vacancy concentration of the Pd/Ce<sub>0.2</sub>Zr<sub>0.8</sub>O<sub>2</sub> catalyst was lower than those of the other catalysts. This difference may be due to the decreased Ce content providing a limited

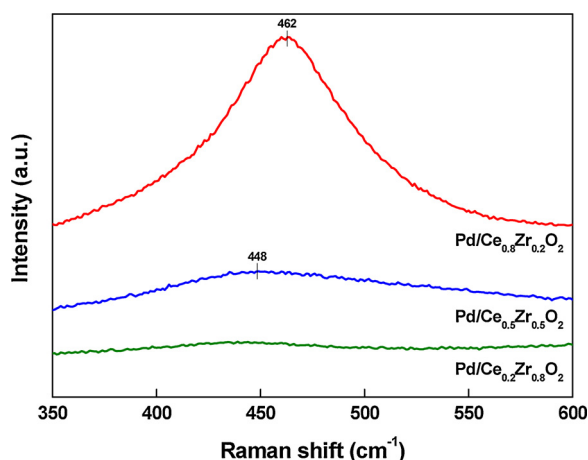


Fig. 3. Raman spectra of Pd/Ce-ZrO<sub>2</sub> catalysts with various Ce/Zr ratios.

supply of oxygen vacancies [49].

### 3.2. Reaction results

The compositions of the reaction products obtained using the prepared catalysts are shown in Table 2. Oleic acid residue was not detected in any of the products, meaning that all the catalysts showed 100% oleic acid conversion. Stearic acid can be formed from hydrogenation of oleic acid, and was the most prevalent single product of the studied reactions [3,51]. Interestingly, the percentage of C<sub>17</sub> hydrocarbons (saturated and unsaturated) was highest in the case of Pd/Ce<sub>0.5</sub>Zr<sub>0.5</sub>O<sub>2</sub> catalyst. These trends are well matched with the concentration of oxygen defects in the catalysts, as calculated by XPS and Raman spectroscopy. Thus, we conclude that the decarboxylation reaction was affected by the oxygen vacancy concentration of the catalysts. Previous reports have found that carboxylic groups that adsorb at the oxygen vacancy sites of nickel catalysts are converted to ketene intermediates (R – COOH → R – COO → R<sub>1</sub> – C = C=O), which are hydrogenated to form aldehydes [20,22]. Aldehydes can be converted to both alcohols and linear hydrocarbons, but neither of these compounds was detected in this study. Furthermore, no C<sub>18</sub> hydrocarbons were detected, which suggests that no hydrodeoxygenation reactions occurred [14,52,53].

In order to confirm the main reaction pathway, micro-GC analysis of the gaseous products was carried out. As shown in Table 3, the main constituent of the product gases was CO<sub>2</sub>. A decarboxylation reaction leads to the removal of a carboxyl group (–COO) from a fatty acid by releasing CO<sub>2</sub>. This clearly indicates that the decarboxylation reaction was the main reaction pathway. In addition, the CO<sub>2</sub> percentage of the product gas was consistent with the extent of decarboxylation. A small amount of CO, which was produced via a decarbonylation reaction, was also presents as part of the product gases. Fig. 4 also shows the percentage of saturated C<sub>17</sub> hydrocarbons (heptadecane) and unsaturated C<sub>17</sub> hydrocarbons (8-heptadecene). Saturated C<sub>17</sub> hydrocarbon was the predominant component of the C<sub>17</sub> hydrocarbon products. This is in agreement with the results from the micro-GC analysis, indicating that most of the oleic acid was converted via decarboxylation. However, we could not determine the other compounds due to the technical limitations connected to micro-GC analysis. It is possible that these by-products are more shorter hydrocarbons (C<sub>4</sub>–C<sub>8</sub>) and oxygenate compounds (due to cracking reaction) [3,13]. The results showed that the Pd/Ce<sub>0.2</sub>Zr<sub>0.8</sub>O<sub>2</sub> catalyst exhibited 3 to 8 times higher amount of by-products than the other two catalysts. In order to find out the reason of the excessive cracking reaction, an NH<sub>3</sub>-TPD analysis was carried out. As shown in Fig. S2, the shapes of the NH<sub>3</sub>-TPD patterns of the prepared catalysts were similar in the temperature range between 100 °C and 500 °C. However, a strong acidic site was detected at 625 °C in the case of the Pd/Ce<sub>0.2</sub>Zr<sub>0.8</sub>O<sub>2</sub> catalyst. Moreover, the Pd/Ce<sub>0.2</sub>Zr<sub>0.8</sub>O<sub>2</sub> catalyst had a higher acidity (701 μmol NH<sub>3</sub>/g<sub>cat</sub>) than both the Pd/Ce<sub>0.5</sub>Zr<sub>0.5</sub>O<sub>2</sub> catalyst (572 μmol NH<sub>3</sub>/g<sub>cat</sub>) and Pd/Ce<sub>0.8</sub>Zr<sub>0.2</sub>O<sub>2</sub> catalysts (401 μmol NH<sub>3</sub>/g<sub>cat</sub>). According to the literature, a strong acidity of a catalyst could induce a cracking reaction [3]. Therefore, it can be assumed that the higher byproduct content in the reaction with the Pd/Ce<sub>0.2</sub>Zr<sub>0.8</sub>O<sub>2</sub> catalyst was due to the strong acidity of the Pd/Ce<sub>0.2</sub>Zr<sub>0.8</sub>O<sub>2</sub> catalyst.

Fig. 5 displays the pressure difference with time on stream over the Pd/Ce<sub>0.5</sub>Zr<sub>0.5</sub>O<sub>2</sub> catalyst, from which the reaction step can be defined. At temperatures up to 100 °C, the initial pressure increase was caused by the thermal cracking of oleic acid and simply the expansion of H<sub>2</sub>. However, when the reaction temperature increased further, to 300 °C, a dramatic pressure drop was observed. The values in Table 2 show that hydrogen is consumed by the conversion of oleic acid (CH<sub>3</sub>(CH<sub>2</sub>)<sub>7</sub>CH = CH(CH<sub>2</sub>)<sub>7</sub>COOH) to stearic acid (CH<sub>3</sub>(CH<sub>2</sub>)<sub>16</sub>COOH). Thus, the hydrogenation reaction occurred before decarboxylation reaction, which occur on the Pd surface. The decarboxylation reaction over Ce<sub>0.5</sub>Zr<sub>0.5</sub>O<sub>2</sub> support without Pd was conducted to check the reaction step. Despite the increasing reaction temperature, a pressure

**Table 2**  
Reaction results over Pd/Ce-ZrO<sub>2</sub> catalysts with various Ce/Zr ratios.

Catalysts	Oleic acid conversion	Stearic acid selectivity	C <sub>17</sub> hydrocarbons selectivity	C <sub>9</sub> –C <sub>16</sub> hydrocarbons selectivity <sup>a</sup>	Oxygen contents	Oxygen removal efficiency <sup>b</sup>	Liquid yield <sup>c</sup> (liquid amount)
Pd/Ce <sub>0.8</sub> Zr <sub>0.2</sub> O <sub>2</sub>	100%	76%	22%	2%	9.4%	18.3%	83.9% (23.1 g)
Pd/Ce <sub>0.5</sub> Zr <sub>0.5</sub> O <sub>2</sub>	100%	63%	34%	3%	9.1%	20.9%	77.0% (21.2 g)
Pd/Ce <sub>0.2</sub> Zr <sub>0.8</sub> O <sub>2</sub>	100%	91%	7%	2%	10.1%	12.1%	88.1% (24.2 g)

<sup>a</sup> Reaction condition: 300 °C, reactant/catalyst = 20/1, 20 bar, H<sub>2</sub> condition.

<sup>a</sup> Saturated hydrocarbons + unsaturated hydrocarbons.

<sup>b</sup> Oxygen contents of oleic acid (reactant) = 11.5%.

<sup>c</sup> Liquid yield expressed as percent (%) is calculated by measuring initial weight of reactant(27.5 g)overweight of liquid product.

**Table 3**  
Micro-GC analysis results over Pd/Ce-ZrO<sub>2</sub> catalysts with various Ce/Zr ratios.

Catalysts	CO <sub>2</sub>	H <sub>2</sub>	CO	CH <sub>4</sub>	Others	Total
Pd/Ce <sub>0.8</sub> Zr <sub>0.2</sub> O <sub>2</sub>	68.6%	19.5%	6.6%	1.1%	4.2%	100.0%
Pd/Ce <sub>0.5</sub> Zr <sub>0.5</sub> O <sub>2</sub>	75.0%	15.0%	7.6%	0.8%	1.6%	100.0%
Pd/Ce <sub>0.2</sub> Zr <sub>0.8</sub> O <sub>2</sub>	56.5%	20.2%	8.0%	2.4%	12.9%	100.0%

<sup>a</sup> Micro-GC analysis results is volume percent.

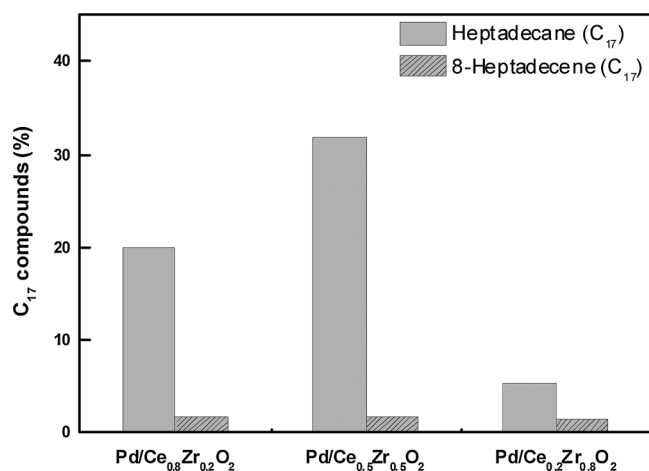


**Fig. 4.** Percentage of saturated C<sub>17</sub> hydrocarbon and unsaturated C<sub>17</sub> hydrocarbon. (Reaction condition: 300 °C, reactant/catalyst = 20/1, 20 bar, H<sub>2</sub> condition).

drop was not observed (Fig. S3). In the case of bare Ce<sub>0.5</sub>Zr<sub>0.5</sub>O<sub>2</sub> support, the pressure increased with the increase in reaction temperature and time. Thus, it can be concluded that the hydrogenation of the oleic acid occurred only on the Pd surface. After the hydrogenation reaction, stearic acid can be converted to heptadecane. After heating was complete, the pressure gradually increased (5.4 bar (0 h) → 8.0 bar (3 h)). One mole of carbon dioxide was generated in the decarboxylation reaction, which is a likely cause of the pressure increase. In addition, a small number of shorter hydrocarbons (C<sub>9</sub>–C<sub>16</sub>) and byproducts were detected, which were likely formed from the cracking of reactant [3]. Fig. 6 shows the selectivities for stearic acid and C<sub>17</sub> hydrocarbons as a function of time on stream over the Pd/Ce<sub>0.5</sub>Zr<sub>0.5</sub>O<sub>2</sub> catalyst. Interestingly, oleic acid was totally converted during temperature rising process. This result is well reflected in the pressure difference with time on stream results shown in Fig. 5. As the initial reaction temperature reached 300 °C, most of the oleic acid is converted to stearic acid. Although the selectivity for the stearic acid at *t* = 0 h was relatively high, it decreased with increasing the time on stream (89%, 0 h → 63%, 3 h). It can be said that the stearic acid was firstly formed before the reaction

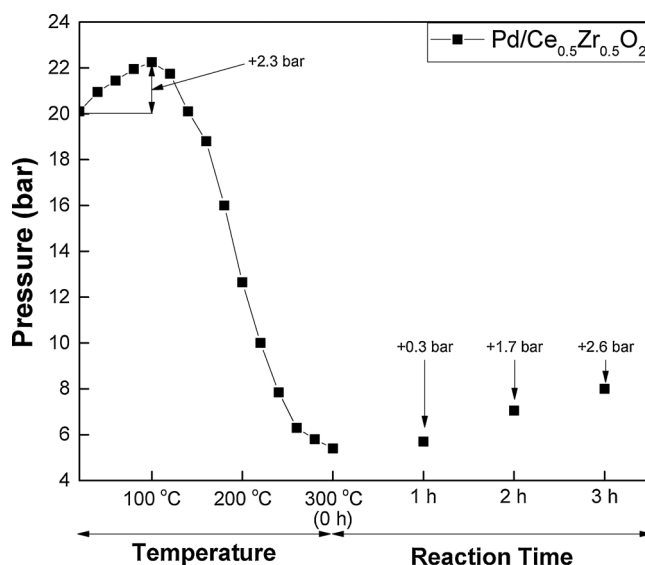


**Fig. 5.** Pressure differences with time on stream over a Pd/Ce<sub>0.5</sub>Zr<sub>0.5</sub>O<sub>2</sub> catalyst. (Reaction condition: 300 °C, reactant/catalyst = 20/1, 20 bar, H<sub>2</sub> condition).

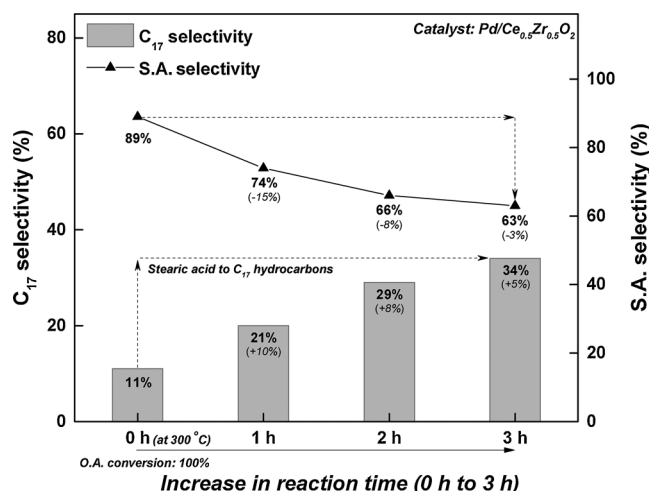


**Fig. 6.** Changes in selectivities for stearic acid and C<sub>17</sub> hydrocarbons observed as a function of time on stream in reaction utilizing the Pd/Ce<sub>0.5</sub>Zr<sub>0.5</sub>O<sub>2</sub> catalyst.

and it was decarboxylated/decarbonylated to afford saturated/unsaturated hydrocarbons.

Elemental analysis was carried out to check the remaining oxygen content of the products, and the results are shown in Table 2 along with the oxygen removal efficiency of the various Pd/Ce-ZrO<sub>2</sub> catalysts. The

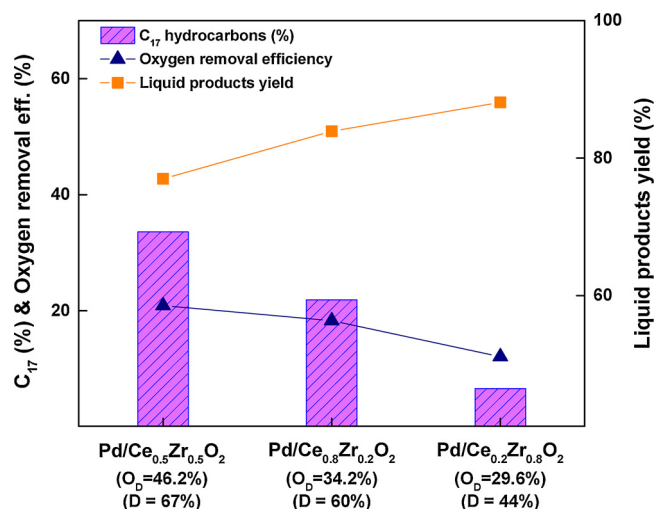


Fig. 7. Relation between the characteristics of catalysts and reaction results. (Reaction condition: 300 °C, reactant/catalyst = 20/1, 20 bar,  $H_2$  condition).

$Pd/Ce_{0.5}Zr_{0.5}O_2$  catalyst exhibited the highest oxygen removal efficiency among the prepared catalysts. According to previous reports, the oxygen removal efficiency and liquid product yield are related to the decarboxylation reaction. The oxygen contained in fatty acids is removed during decarboxylation in the form of carbon dioxide [3,12,54]. The liquid product yields of the various Pd/Ce-Zr $O_2$  catalysts are shown in Table 2. The  $Pd/Ce_{0.5}Zr_{0.5}O_2$  catalyst also exhibited the lowest liquid product yield among the tested catalysts. The liquid product yield increased in the order:  $Pd/Ce_{0.5}Zr_{0.5}O_2$  (77.0%) <  $Pd/Ce_{0.8}Zr_{0.2}O_2$  (83.9%) <  $Pd/Ce_{0.2}Zr_{0.8}O_2$  (88.1%). The selectivity for  $C_{17}$  hydrocarbons, liquid product yield, and oxygen removal efficiency are compared for each catalyst in Fig. 7. The decarboxylation reaction (selectivity for  $C_{17}$  hydrocarbons) influences the liquid product yield and oxygen removal efficiency. In addition, catalytic performance was strongly affected by the oxygen vacancy concentration and Pd dispersion. As shown in Table 3, the sum of  $CO_2$ ,  $H_2$  (just residue), and CO was almost 95%, except for the case of the  $Pd/Ce_{0.2}Zr_{0.8}O_2$  catalyst, which contained 12.9% thermal and catalytic cracking-derived compounds. Thus, it can be concluded that the gas yield was almost equal to the oxygen removal efficiency. Table S1 shows the differences between these two factors. Note, that small differences may occur due to analytical errors. Therefore, it was concluded that the oxygen removal efficiency was in accordance with the extent of decarboxylation.

A cycling test was conducted to check the stability of  $Pd/Ce_{0.5}Zr_{0.5}O_2$  catalyst (Table 4). Interestingly, all the used catalysts showed 100% oleic acid conversion. However, their selectivity for  $C_{17}$  compounds decreased as the number of usage cycles increased, and the stearic acid selectivity increased as the  $C_{17}$  selectivity decreased. BET, CO-chemisorption, and XPS analyses of the recycled catalysts were conducted to determine the cause of the observed deactivation (Table 4 and Fig. 8). Fig. 8 shows the O 1s spectra of the used  $Pd/Ce_{0.5}Zr_{0.5}O_2$  catalyst. Three kinds of oxygen species were detected in the XPS

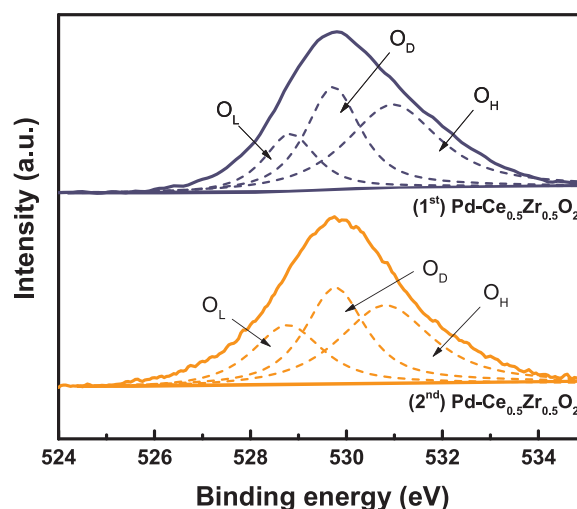


Fig. 8. O 1s XPS spectra of used  $Pd/Ce_{0.5}Zr_{0.5}O_2$  catalysts.

spectrum, as for the fresh  $Pd/Ce_{0.5}Zr_{0.5}O_2$  catalyst. The positions of the deconvoluted peaks are similar to those of the fresh  $Pd/Ce_{0.5}Zr_{0.5}O_2$  catalyst. The quantitative XPS elemental analyses of the O 1s peak of the used  $Pd/Ce_{0.5}Zr_{0.5}O_2$  catalysts are shown in Table 4. The concentration of surface oxygen defects of the used  $Pd/Ce_{0.5}Zr_{0.5}O_2$  catalysts decreased as the number of uses increased (46.2% → 34.9% → 30.4%). This result clearly shows that the oxygen vacancy concentration is related to the activity of the catalyst for the decarboxylation reaction. Especially, a dramatic reduction of BET surface area ( $122 \text{ m}^2/\text{g} \rightarrow 42 \text{ m}^2/\text{g} \rightarrow 24 \text{ m}^2/\text{g}$ ) and Pd dispersion (67% → 5% (−93%) → 2% (−97%)) are a main factor in catalyst deactivation. We suggest that the oxygen vacancies are blocked by strongly adsorbed carboxylic groups, thereby decreasing the concentration of oxygen vacancies. Table 4 compares the characteristics of the fresh and used  $Pd/Ce_{0.5}Zr_{0.5}O_2$  catalysts. The BET surface area of  $Pd/Ce_{0.5}Zr_{0.5}O_2$  catalyst decreased by 65% and 80% after each subsequent reaction. The Pd dispersion of  $Pd/Ce_{0.5}Zr_{0.5}O_2$  catalyst also decreased to 5% and 2% after recycling. The CO-chemisorption data indicates that significant Pd sintering is also observed. Thus, we conclude that the causes of catalyst deactivation are mainly Pd sintering, decreases in BET surface area and Pd dispersion, and the partial reduction in oxygen vacancy concentration.

In this study, the Pd/Ce-Zr $O_2$  catalyst activity was affected by the Ce/Zr ratio. The Ce/Zr ratio affects the formation of oxygen vacancy concentration, which is the effect on the decarboxylation reaction. We also found that the decarboxylation reaction was the main reaction pathway in this study. Thus, we propose the reaction step in this reaction is as follows. First, oleic acid is hydrogenated to stearic acid. Second, stearic acid is dissociated with carboxylate compounds (R-COO) and hydrogen, which occurred at the oxygen vacancy sites and Pd surface. Thus, the oxygen vacancy concentration and Pd dispersion (active Pd particle size) have a strong influence on this reaction. After adsorption, C–C scission occurs and the resultant products are hydrogenated to produce linear hydrocarbons and carbon dioxide.

Table 4  
Characteristics and reaction results of fresh and used  $Pd/Ce_{0.5}Zr_{0.5}O_2$  catalysts.

Catalysts	Oleic acid conversion	Stearic acid selectivity	$C_{17}$ hydrocarbons selectivity	BET S.A. ( $\text{m}^2/\text{g}$ ) <sup>a</sup>	Pd dispersion <sup>b</sup>	Active Pd particle size (nm) <sup>b</sup>	$O_D / (O_L + O_D + O_H)$
(Fresh) $Pd/Ce_{0.8}Zr_{0.2}O_2$	100%	63%	34%	122	67%	1.7	46.2%
(1 <sup>st</sup> ) $Pd/Ce_{0.5}Zr_{0.5}O_2$	100%	81%	17%	42 (−65%)	5% (−93%)	24.9	34.9%
(2 <sup>nd</sup> ) $Pd/Ce_{0.2}Zr_{0.8}O_2$	100%	94%	5%	24 (−80%)	2% (−97%)	72.3	30.4%

<sup>a</sup> Reaction condition: 300 °C, reactant/catalyst = 20/1, 20 bar,  $H_2$  condition.

<sup>a</sup> Estimated from  $N_2$  adsorption at −196 °C.

<sup>b</sup> Estimated from CO-chemisorption.

Finally, both are desorbed.

#### 4. Conclusions

The catalytic performance of Pd/Ce-ZrO<sub>2</sub> catalysts depends on the Ce/Zr ratio. The formation of oxygen vacancy concentration was also affected by the Ce/Zr ratio. Moreover, the oxygen vacancy concentration has a strong effect on the decarboxylation reaction. The Pd/Ce<sub>0.5</sub>Zr<sub>0.5</sub>O<sub>2</sub> catalyst shows the highest selectivity for C<sub>17</sub> compounds and oxygen removal efficiency among the prepared catalysts. The highest catalytic activity is found with the catalyst with the highest oxygen vacancy concentration. The Pd dispersion also has a strong effect on the catalytic activity. The causes of catalyst deactivation are mainly Pd sintering, a decrease of BET surface area and Pd dispersion, and partially the loss of oxygen vacancies. Additionally, the reaction proceeded mainly via a decarboxylation reaction pathway.

#### Acknowledgments

This work was supported by the National Research Foundation of Korea (NRF) grant funded by the Korea government (MSIP) (2017R1A2B4007145).

#### Appendix A. Supplementary data

Supplementary material related to this article can be found, in the online version, at doi:<https://doi.org/10.1016/j.apcata.2018.07.005>.

#### References

- J.P. Ford, N. Thapaliya, M.J. Kelly, W.L. Roberts, H.H. Lamb, *Energy Fuels* 27 (2013) 7489–7496.
- J.G. Immer, M.J. Kelly, H.H. Lamb, *Appl. Catal. A: Gen.* 375 (2010) 134–139.
- J.-O. Shim, D.-W. Jeong, W.-J. Jang, K.-W. Jeon, S.-H. Kim, B.-H. Jeon, H.-S. Roh, J.-G. Na, Y.-K. Oh, S.S. Han, C.H. Ko, *Catal. Commun.* 67 (2015) 16–20.
- S. Dutta, B. Saha, *ACS Catal.* 7 (2017) 5491–5499.
- P.M. Mortensen, J.-D. Grunwaldt, P.A. Jensen, K.G. Knudsen, A.D. Jensen, *Appl. Catal. A: Gen.* 407 (2011) 1–19.
- G. Bauer, S. Lima, J. Chenevard, M. Sugnaux, F. Fischer, *ACS Sustain. Chem. Eng.* 5 (2017) 1931–1937.
- L. Yang, K.L. Tate, J.B. Jasinski, M.A. Carreon, *ACS Catal.* 5 (2015) 6497–6502.
- B. Smith, H.G. Greenwell, A. Whiting, *Energy Environ. Sci.* 2 (2009) 262–271.
- G. Knothe, *Fuel Process. Technol.* 86 (2005) 1059–1070.
- M.J. Ramos, C.M. Fernandez, A. Casas, L. Rodriguez, A. Perez, *Bioresour. Technol.* 100 (2009) 261–268.
- M. Snåre, I. Kubičková, P. Mäki-Arvela, K. Eränen, D.Y. Murzin, *Ind. Eng. Chem. Res.* 45 (2006) 5708–5715.
- J.-G. Na, J.K. Han, Y.-K. Oh, J.-H. Park, T.S. Jung, S.S. Han, H.C. Yoon, S.H. Chung, J.-N. Kim, C.H. Ko, *Catal. Today* 185 (2012) 313–317.
- M. Arendt, T. Nonnen, W.F. Hoelderich, J. Fischer, J. Groos, *Appl. Catal. A: Gen.* 399 (2011) 198–204.
- M. Snåre, I. Kubičková, P. Mäki-Arvela, K. Eränen, J. Wärnå, D.Y. Murzin, *Chem. Eng. J.* 134 (2007) 29–34.
- M. Ahmadi, E.E. Macias, J.B. Jasinski, P. Ratnasamy, M.A. Carreon, *J. Mol. Catal. A: Chem.* 386 (2014) 14–19.
- H.-S. Roh, I.-H. Eum, D.-W. Jeong, B.E. Yi, J.-G. Na, C.H. Ko, *Catal. Today* 164 (2011) 457–460.
- J.-O. Shim, D.-W. Jeong, W.-J. Jang, K.-W. Jeon, B.-H. Jeon, S.-H. Kim, H.-S. Roh, J.-G. Na, S.S. Han, C.H. Ko, *J. Nanosci. Nanotechnol.* 16 (2016) 4587–4592.
- Y. Wang, J. Wu, S. Wang, *RSC Adv.* 3 (2013) 12635–12640.
- V.A. Yakovlev, S.A. Khromova, O.V. Sherstyuk, V.O. Dundich, D.Y. Ermakov, V.M. Novopashina, M. Yu, O. Lebedev, V.N. Bulavchenko, Parmon, *Catal. Today* 144 (2009) 362–366.
- B. Peng, X. Yuan, C. Zhao, J.A. Lercher, *J. Am. Chem. Soc.* 134 (2012) 9400–9405.
- E. Meller, U. Green, Z. Aizenshtat, Y. Sasson, *Fuel* 133 (2014) 89–95.
- B. Peng, C. Zhao, S. Kasakov, S. Foraita, J.A. Lercher, *Chem. Eur. J.* 19 (2013) 4732–4741.
- P. Mäki-Arvela, I. Kubičková, M. Snåre, K. Eränen, D.Y. Murzin, *Energy Fuels* 21 (2007) 30–41.
- S. Lestari, I. Simakova, A. Tokarev, P. Mäki-Arvela, K. Eränen, D.Y. Murzin, *Catal. Lett.* 122 (2008) 247–251.
- S. Lestari, P. Mäki-Arvela, K. Eränen, J. Beltramini, G.Q. Max Lu, D.Y. Murzin, *Catal. Lett.* 130 (2009) 48–51.
- I. Simakova, O. Simakova, P. Mäki-Arvela, A. Simakov, M. Estrada, D.Y. Murzin, *Appl. Catal. A: Gen.* 355 (2009) 100–108.
- S. Lestari, P. Mäki-Arvela, H. Bernas, O. Simakova, R. Sjöholm, J. Beltramini, G.Q. Max Lu, J. Myllyoja, I. Simakova, D.Y. Murzin, *Energy Fuels* 23 (2009) 3842–3845.
- I. Simakova, B. Rozmyslowicz, O. Simakova, P. Mäki-Arvela, A. Simakov, D.Y. Murzin, *Top. Catal.* 54 (2011) 460–466.
- J.P. Ford, J.G. Immer, H.H. Lamb, *Top. Catal.* 55 (2012) 175–184.
- J.-O. Shim, D.-W. Jeong, W.-J. Jang, K.-W. Jeon, B.-H. Jeon, S.-Y. Cho, H.-S. Roh, J.-G. Na, C.H. Ko, Y.-K. Oh, S.S. Han, *Renew. Energy* 65 (2014) 36–40.
- J.-O. Shim, Y.-J. Hong, H.-S. Na, W.-J. Jang, Y.C. Kang, H.-S. Roh, *ACS Appl. Mater. Interfaces* 8 (2016) 17239–17244.
- W.-J. Jang, H.-M. Kim, J.-O. Shim, S.-Y. Yoo, K.-W. Jeon, H.-S. Na, Y.-L. Lee, D.-W. Jeong, J.W. Bae, I.W. Nah, H.-S. Roh, *Green Chem.* 20 (2018) 1621–1633.
- W.-J. Jang, D.-W. Jeong, J.-O. Shim, H.-S. Roh, I.H. Son, S.J. Lee, *Int. J. Hydrogen Energy* 38 (2013) 4508–4512.
- H.-S. Roh, I.-H. Eum, D.-W. Jeong, *Renew. Energy* 42 (2012) 212–216.
- W.-J. Jang, D.-W. Jeong, J.-O. Shim, H.-M. Kim, W.-B. Han, J.W. Bae, H.-S. Roh, *Renew. Energy* 79 (2015) 91–95.
- R. Pellegrini, G. Leofanti, G. Agostini, E. Groppo, M. Rivallan, C. Lamberti, *Langmuir* 25 (2009) 6476–6485.
- P. Trogadas, J. Parrondo, V. Ramani, *ACS Appl. Mater. Interfaces* 4 (2012) 5098–5102.
- J.-O. Shim, H.-S. Na, A. Jha, W.-J. Jang, D.-W. Jeong, I.W. Nah, B.-H. Jeon, H.-S. Roh, *Chem. Eng. J.* 306 (2016) 908–915.
- D.-W. Jeong, H.S. Potdar, J.-O. Shim, W.-J. Jang, H.-S. Roh, *Int. J. Hydrogen Energy* 38 (2013) 4502–4507.
- Z. Sun, D.Y. Lu, F.N. Ridha, R.W. Hughes, D. Filippou, *Appl. Energy* 195 (2017) 303–315.
- L. Qi, Q. Yu, Y. Dai, C. Tang, L. Liu, H. Zhang, F. Gao, L. Dong, Y. Chen, *Appl. Catal. B: Environ.* 119–120 (2012) 308–320.
- H.-S. Roh, H.S. Potdar, K.-W. Jun, *Catal. Today* 93–95 (2004) 39–44.
- W. Chen, R. Ran, D. Weng, X. Wu, J. Zhong, A. Zhu, S. Han, *J. Mater. Sci.* 50 (2015) 6268–6276.
- M. Piumetti, S. Bensaid, T. Andana, N. Russo, R. Pirone, D. Fino, *Appl. Catal. B: Environ.* 205 (2017) 455–468.
- F. Morfin, T.-S. Nguyen, J.-L. Rousset, L. Piccolo, *Appl. Catal. B: Environ.* 197 (2016) 2–13.
- Z.-Y. Pu, J.-Q. Lu, M.-F. Luo, Y.-L. Xie, *J. Phys. Chem. C* 111 (2007) 18695–18702.
- M. Shen, L. Lv, J. Wang, J. Zhu, Y. Huang, *J. Wang, Chem. Eng. J.* 255 (2014) 40–48.
- B. Malleshram, P. Sudarsanam, B.V.S. Reddy, B.M. Reddy, *Appl. Catal. B: Environ.* 181 (2016) 47–57.
- L. Yang, X. Yang, R. Zhou, *J. Phys. Chem. C* 120 (2016) 2712–2723.
- T.H. Vuong, J. Radnik, E. Kondratenko, M. Schneider, U. Armbruster, A. Brückner, *Appl. Catal. B: Environ.* 197 (2016) 159–167.
- A. Dragu, S. Kinayyigit, E.J. García-Suárez, M. Florea, E. Stepan, S. Velea, L. Tanase, V. Collière, K. Philippot, P. Granger, V.I. Parvulescu, *Appl. Catal. A: Gen.* 504 (2015) 81–91.
- K.A. Roger, Y. Zheng, *ChemSusChem* 9 (2016) 1750–1772.
- M. Snåre, I. Kubičková, P. Mäki-Arvela, D. Chichova, K. Eränen, D.Y. Murzin, *Fuel* 87 (2008) 933–945.
- J.-G. Na, B.E. Yi, J.N. Kim, K.B. Yi, S.-Y. Park, J.-H. Park, J.-N. Kim, C.H. Ko, *Catal. Today* 156 (2010) 44–48.